

# Discontinuous Galerkin methods for Maxwell's equations in Drude metamaterials on unstructured meshes

Cengke Shi, \*      Jichun Li, †      Chi-Wang Shu ‡

April 8, 2018

**Abstract.** In this follow-up work, we extend the discontinuous Galerkin (DG) methods previously developed on rectangular meshes [18] to triangular meshes. The DG schemes in [18] are both optimally convergent and energy conserving. However, as we shall see in the numerical results section, the DG schemes on triangular meshes only have suboptimal convergence rate. We prove the energy conservation and an error estimate for the semi-discrete schemes. The stability of the fully discrete scheme is proved and its error estimate is stated. We present extensive numerical results with convergence consistent of our error estimate, and simulations of wave propagation in Drude metamaterials to demonstrate the flexibility of triangular meshes.

## 1 Introduction

Since the first successful construction of metamaterials with double negative permittivity and permeability in 2000 by Smith et al. [23], they have attracted a great interest. Metamaterial has applications in many areas such as invisibility cloak design (e.g. [25, 29]), velocity-selective particle detections by the reversed Cherenkov radiation (e.g. [5, 14]) and sub-wavelength imaging (e.g. [1]). Numerical simulation of electromagnetic wave propagation in metamaterials plays a very important role in these investigations, and requires solving a system of more complicated time domain Maxwell's equations than the standard Maxwell's equations in free space. Though there are many excellent papers for solving Maxwell's equations in free space (see [3, 7, 13, 15, 17, 20, 21, 30] and references therein), published works on efficient and rigorous numerical methods for metamaterial Maxwell's equations are still quite limited [2, 4, 6, 19, 24, 28].

The discontinuous Galerkin (DG) method was initially introduced in 1973 by Reed and Hill [22] for solving a neutron transport equation. The work of Cockburn and Shu [9, 10] on Runge-Kutta DG (RKDG) methods for solving linear and nonlinear time dependent hyperbolic partial differential equations (PDEs), in which space is discretized by DG methods and time by Runge-Kutta methods (other time discretization methods are of course also possible, such as the leap frog method adopted in this paper), has facilitated the rapid advance and application of DG methods. Over the past four decades, various DG methods have been proposed for solving different PDEs. The

---

\*Division of Applied Mathematics, Brown University, Providence, RI 02912, USA. (cengke.shi@brown.edu)

†Department of Mathematical Sciences, University of Nevada Las Vegas, Las Vegas, Nevada 89154-4020, USA. (jichun.li@unlv.edu) Research supported by NSF grant DMS-1416742.

‡Division of Applied Mathematics, Brown University, Providence, RI 02912, USA. (shu@dam.brown.edu). Research supported by ARO grant W911NF-15-1-0226 and NSF grant DMS-1719410.

popularity of DG methods is due to their nice features such as local solvability, flexibility in  $h$ - $p$  adaptivity, and efficiency in parallel implementation. Also relevant to our schemes studied in this paper, especially the choice of the alternating fluxes, we should mention the so-called local discontinuous Galerkin (LDG) method, which was introduced by Cockburn and Shu [11] for solving time-dependent convection-diffusion systems and was used in [26] for solving second-order hyperbolic equations. For more details on the algorithm design, analysis, implementation and application of DG and LDG schemes for solving time-dependent PDEs, readers can consult the review articles [12, 27] and the references therein.

Li and Hesthaven [16] developed a DG scheme with central flux for Maxwell's equations in Drude metamaterials, and the scheme is energy conserving but converges suboptimally. In our previous work [18], we developed a energy conserving and optimal DG scheme by using alternating flux on rectangular meshes. As a follow-up work of [18], here we develop a DG scheme with alternating flux on triangular meshes. This DG scheme conserves the energy but has a suboptimal convergence rate. The major advantage of developing a DG scheme on triangular meshes is that we can use it to simulate the backward wave propagation phenomena in complex domains.

The rest of the paper is organized as follows. In Sect. 2, we first present the governing equations for wave propagation in Drude metamaterials. In Sect. 3, we present the semi-discrete DG method, and prove its stability along with a suboptimal error estimate in the  $L^2$  norm. Then in Sect. 4, we propose a fully discrete DG method with leap-frog time discretization. Stability analysis of the scheme is carried out. The convergence result is stated, but the lengthy technical proof is skipped as it mostly follows the line of the proof of the semi-discrete case. Sect. 5 includes numerical experiments demonstrating the suboptimal convergence rates of the proposed DG method. Wave propagation simulation in complex regions mixed with Drude metamaterials is also included in this section. Finally, we conclude the paper in Sect. 6.

## 2 The governing equations

As in [18], we only consider the transverse-electric mode with respect to  $z$  in two dimensions (2-D), i.e., the so-called  $TE_z$  mode, which involves only the electric field  $\mathbf{E} = (E_x, E_y)$ , the magnetic field  $\mathbf{H} = H_z$ , the induced electric current  $\mathbf{J} = (J_x, J_y)$ , and the induced magnetic current  $\mathbf{K} = K_z$ . Here the subindices  $x, y$  and  $z$  denote the components in the  $x, y$  and  $z$  directions, respectively. More specifically, the governing equations of the  $TE_z$  Drude model can be written as:

$$\epsilon_0 \frac{\partial E_x}{\partial t} = \frac{\partial H_z}{\partial y} - J_x, \quad (1)$$

$$\epsilon_0 \frac{\partial E_y}{\partial t} = -\frac{\partial H_z}{\partial x} - J_y, \quad (2)$$

$$\mu_0 \frac{\partial H_z}{\partial t} = -\frac{\partial E_y}{\partial x} + \frac{\partial E_x}{\partial y} - K_z, \quad (3)$$

$$\frac{1}{\epsilon_0 \omega_{pe}^2} \frac{\partial J_x}{\partial t} + \frac{\Gamma_e}{\epsilon_0 \omega_{pe}^2} J_x = E_x, \quad (4)$$

$$\frac{1}{\epsilon_0 \omega_{pe}^2} \frac{\partial J_y}{\partial t} + \frac{\Gamma_e}{\epsilon_0 \omega_{pe}^2} J_y = E_y, \quad (5)$$

$$\frac{1}{\mu_0 \omega_{pm}^2} \frac{\partial K_z}{\partial t} + \frac{\Gamma_m}{\mu_0 \omega_{pm}^2} K_z = H_z, \quad (6)$$

where  $\epsilon_0$  is the vacuum permittivity,  $\mu_0$  is the vacuum permeability,  $\omega_{pe} > 0$  and  $\omega_{pm} > 0$  are the electric and magnetic plasma frequencies respectively, and  $\Gamma_e \geq 0$  and  $\Gamma_m \geq 0$  are the electric and magnetic damping frequencies respectively. To make the model problem (1)-(6) well-posed, we assume that the problem (1)-(6) satisfies the following initial conditions

$$\mathbf{E}(\mathbf{x}, 0) = \mathbf{E}_0(\mathbf{x}), \quad \mathbf{H}(\mathbf{x}, 0) = \mathbf{H}_0(\mathbf{x}), \quad \mathbf{J}(\mathbf{x}, 0) = \mathbf{J}_0(\mathbf{x}), \quad \mathbf{K}(\mathbf{x}, 0) = \mathbf{K}_0(\mathbf{x}), \quad (7)$$

and the perfect conduct (PEC) boundary condition

$$E_x(x, y, t)|_{y=c,d} = 0, \quad E_y(x, y, t)|_{x=a,b} = 0. \quad (8)$$

For simplicity, we consider solving (1)-(6) on a rectangular type physical domain  $\Omega = [a, b] \times [c, d]$ , which is discretized by a triangular mesh,  $\Omega = \cup_{e \in \mathcal{T}_h} e$ .  $\mathcal{T}_h$  represents a triangulation on  $\Omega$  with mesh size  $h$  defined as the largest diameter of all triangles. The time domain  $[0, T]$  is discretized into  $N_t + 1$  uniform intervals by discrete times  $0 = t_0 < t_1 < \dots < t_{N_t+1} = T$ , where  $t_n = n \cdot \tau$ , and the time step size  $\tau = \frac{T}{N_t+1}$ .

The finite element space  $V_h^k$  is chosen as piecewise polynomials of degree at most  $k$  on every element  $e$ , i.e.,

$$V_h^k = \{v : v|_e \in P_k(e), \quad \forall e \in \mathcal{T}_h\}, \quad (9)$$

where  $P_k$  is the space of polynomial of degree up to  $k$ . To get the error estimate, we need some regularity conditions on the triangulation similar to those in chapter 3 of [8]:

- 1 There exists a constant  $\theta_0 \geq 0$ , such that all angles in the triangles are larger than  $\theta_0$ .
- 2 There exists a constant  $C$ , such that: ( $h_e$  denotes the diameter of triangle  $e$ )

$$\max_{e \in \mathcal{T}_h} h_e < C \min_{e \in \mathcal{T}_h} h_e$$

For the corresponding variable  $u$  we denote its numerical solution  $u_h$ , which belongs to the finite element space  $V_h^k$ . Note that functions in  $V_h^k$  are allowed to have discontinuities across element interfaces. In the line integral over the boundary of a cell, we denote  $u_h^{(in)}$  as the value of  $u_h$  taken from inside of that cell, and  $u_h^{(out)}$  from the neighboring cell sharing that boundary. We denote by  $\|\cdot\|$  the  $L^2$  norm over the domain  $\Omega$ .

### 3 The semi-discrete DG method

The DG method for (1)-(6) can be formulated as follows: Find  $E_{xh}, E_{yh}, H_{zh}, J_{xh}, J_{yh}, K_{zh} \in C^1([0, T]; V_h^k)$  such that

$$\epsilon_0 \int_e \frac{\partial E_{xh}}{\partial t} \phi_x + \int_e H_{zh} \frac{\partial \phi_x}{\partial y} - \int_{\partial e} \hat{H}_{zh} \phi_x^{(in)} n_y^{(in)} + \int_e J_{xh} \phi_x = 0, \quad (10)$$

$$\epsilon_0 \int_e \frac{\partial E_{yh}}{\partial t} \phi_y - \int_e H_{zh} \frac{\partial \phi_y}{\partial x} + \int_{\partial e} \hat{H}_{zh} \phi_y^{(in)} n_x^{(in)} + \int_e J_{yh} \phi_y = 0, \quad (11)$$

$$\mu_0 \int_e \frac{\partial H_{zh}}{\partial t} \psi - \int_e E_{yh} \frac{\partial \psi}{\partial x} + \int_e E_{xh} \frac{\partial \psi}{\partial y} + \int_{\partial e} (\hat{E}_{yh} n_x^{(in)} - \hat{E}_{xh} n_y^{(in)}) \psi^{(in)} + \int_e K_{zh} \psi = 0, \quad (12)$$

$$\frac{1}{\epsilon_0 \omega_{pe}^2} \int_e \frac{\partial J_{xh}}{\partial t} u_1 + \frac{\Gamma_e}{\epsilon_0 \omega_{pe}^2} \int_e J_{xh} u_1 - \int_e E_{xh} u_1 = 0, \quad (13)$$

$$\frac{1}{\epsilon_0 \omega_{pe}^2} \int_e \frac{\partial J_{yh}}{\partial t} u_2 + \frac{\Gamma_e}{\epsilon_0 \omega_{pe}^2} \int_e J_{yh} u_2 - \int_e E_{yh} u_2 = 0, \quad (14)$$

$$\frac{1}{\mu_0 \omega_{pm}^2} \int_e \frac{\partial K_{zh}}{\partial t} v + \frac{\Gamma_m}{\mu_0 \omega_{pm}^2} \int_e K_{zh} v - \int_e H_{zh} v = 0, \quad (15)$$

for all test functions  $\phi_x, \phi_y, \psi, u_1, u_2, v \in V_h^k$  and all triangle cells  $e \in \mathcal{T}_h$ .  $\hat{H}_{zh}, \hat{E}_{yh}, \hat{E}_{xh}$  are the cell boundary terms obtained from integration by parts, and they are the so-called numerical fluxes. In the line integration over  $\partial e$ ,  $\mathbf{n}^{(in)} = (n_x^{(in)}, n_y^{(in)})$  is the unit normal vector pointing towards the outside of the element  $e$ .

We choose the alternating flux as in [18]. To define alternating flux in a triangulation, we need to first choose a fix direction  $\boldsymbol{\beta}$  that is not parallel with any triangle boundary edge. On each edge, we can define the “right” and “left” side with respect to  $\boldsymbol{\beta}$ . On each side there is an outward normal direction,  $\mathbf{n}$ , orthogonal to the edge. We define a side is the “right” side if  $\mathbf{n} \cdot \boldsymbol{\beta} < 0$ . The alternating flux is defined as always choosing  $E_{xh}$  and  $E_{yh}$  on the “right” side and  $H_{zh}$  on the “left” side:

$$\hat{E}_{xh} = E_{xh}^R, \quad (16)$$

$$\hat{E}_{yh} = E_{yh}^R, \quad (17)$$

$$\hat{H}_{zh} = H_{zh}^L. \quad (18)$$

A more detailed explanation of alternating flux for triangulation can be found in [27]. It is easy to check that the definition of the alternating flux in [18] is a special case of the one here with  $\boldsymbol{\beta} = (1, 1)$ . If we adopt a periodic boundary condition, the above definition of alternating flux is enough. However, to satisfy the PEC boundary condition in (8), we take

$$\hat{E}_{xh} = 0, \text{ on } y = c, d, \quad (19)$$

$$\hat{E}_{yh} = 0, \text{ on } x = a, b, \quad (20)$$

$$\hat{H}_{zh} = H_{zh}^{(in)}, \text{ on } \partial\Omega. \quad (21)$$

### 3.1 The stability analysis

In this subsection, we present the stability analysis for our scheme.

First, let us look at the stability for the governing equations. Multiplying the governing equations (1)–(6) by  $E_x, E_y, H_z, J_x, J_y, K_z$ , respectively, then integrating over the space and time domain  $\Omega \times [0, t]$ , summing up the resultants, and using the 2D PEC boundary condition (8), we can easily obtain the energy identity:

$$\begin{aligned} & \left[ \epsilon_0 (\|E_x\|^2 + \|E_y\|^2) + \mu_0 \|H_z\|^2 + \frac{1}{\epsilon_0 \omega_{pe}^2} (\|J_x\|^2 + \|J_y\|^2) + \frac{1}{\mu_0 \omega_{pm}^2} \|K_z\|^2 \right] (t) \\ & + \int_0^t \left[ \frac{2\Gamma_e}{\epsilon_0 \omega_{pe}^2} (\|J_x\|^2 + \|J_y\|^2) + \frac{2\Gamma_m}{\mu_0 \omega_{pm}^2} \|K_z\|^2 \right] (s) ds \end{aligned}$$

$$= \left[ \epsilon_0(\|E_x\|^2 + \|E_y\|^2) + \mu_0\|H_z\|^2 + \frac{1}{\epsilon_0\omega_{pe}^2}(\|J_x\|^2 + \|J_y\|^2) + \frac{1}{\mu_0\omega_{pm}^2}\|K_z\|^2 \right] (0). \quad (22)$$

Below we will show that the solution of our proposed semi-discrete DG method satisfies a similar energy identity as in the continuous level (22).

**Theorem 3.1.** *The semi-discrete DG method (10)-(15) with alternating fluxes (16)-(21) satisfies the following energy identity: For any  $t \geq 0$ :*

$$\begin{aligned} & \left[ \epsilon_0(\|E_{xh}\|^2 + \|E_{yh}\|^2) + \mu_0\|H_{zh}\|^2 + \frac{1}{\epsilon_0\omega_{pe}^2}(\|J_{xh}\|^2 + \|J_{yh}\|^2) + \frac{1}{\mu_0\omega_{pm}^2}\|K_{zh}\|^2 \right] (t) \\ & + \int_0^t \left[ \frac{2\Gamma_e}{\epsilon_0\omega_{pe}^2}(\|J_{xh}\|^2 + \|J_{yh}\|^2) + \frac{2\Gamma_m}{\mu_0\omega_{pm}^2}\|K_{zh}\|^2 \right] (s) ds \\ & = \left[ \epsilon_0(\|E_{xh}\|^2 + \|E_{yh}\|^2) + \mu_0\|H_{zh}\|^2 + \frac{1}{\epsilon_0\omega_{pe}^2}(\|J_{xh}\|^2 + \|J_{yh}\|^2) + \frac{1}{\mu_0\omega_{pm}^2}\|K_{zh}\|^2 \right] (0). \end{aligned} \quad (23)$$

*Proof.* Taking  $\phi_x = E_{xh}, \phi_y = E_{yh}, \psi = H_{zh}, u_1 = J_{xh}, u_2 = J_{yh}, v = K_{zh}$  in (10)-(15), respectively, adding the resultants together over all cells, we have

$$\begin{aligned} & \frac{1}{2} \frac{d}{dt} \int_{\Omega} \left[ \epsilon_0(|E_{xh}|^2 + |E_{yh}|^2) + \mu_0|H_{zh}|^2 + \frac{1}{\epsilon_0\omega_{pe}^2}(|J_{xh}|^2 + |J_{yh}|^2) + \frac{1}{\mu_0\omega_{pm}^2}|K_{zh}|^2 \right] \\ & + \int_{\Omega} \left[ \frac{\Gamma_e}{\epsilon_0\omega_{pe}^2}(|J_{xh}|^2 + |J_{yh}|^2) + \frac{\Gamma_m}{\mu_0\omega_{pm}^2}|K_{zh}|^2 \right] \\ & + \sum_{e \in \mathcal{T}_h} \int_{\partial e} \left( -\hat{H}_{zh} E_{xh}^{(in)} n_y^{(in)} + \hat{H}_{zh} E_{yh}^{(in)} n_x^{(in)} + H_{zh}^{(in)} \hat{E}_{yh} n_x^{(in)} - H_{zh}^{(in)} \hat{E}_{xh} n_y^{(in)} \right) \\ & + \sum_{e \in \mathcal{T}_h} \int_e \left( H_{zh} \frac{\partial E_{xh}}{\partial y} - H_{zh} \frac{\partial E_{yh}}{\partial x} - E_{yh} \frac{\partial H_{zh}}{\partial x} + E_{xh} \frac{\partial H_{zh}}{\partial y} \right) = 0. \end{aligned} \quad (24)$$

Using integration by parts, the terms in the last two lines of (24) become  $F_x - F_y$ , where

$$F_x = \sum_{e \in \mathcal{T}_h} \int_{\partial e} \left( H_{zh}^{(in)} E_{xh}^{(in)} n_y^{(in)} - \hat{H}_{zh} E_{xh}^{(in)} n_y^{(in)} - H_{zh}^{(in)} \hat{E}_{xh} n_y^{(in)} \right), \quad (25)$$

$$F_y = \sum_{e \in \mathcal{T}_h} \int_{\partial e} \left( H_{zh}^{(in)} E_{yh}^{(in)} n_x^{(in)} - \hat{H}_{zh} E_{yh}^{(in)} n_x^{(in)} - H_{zh}^{(in)} \hat{E}_{yh} n_x^{(in)} \right). \quad (26)$$

By grouping terms by sides of triangles instead of triangles, we have:

$$\begin{aligned} F_x &= \sum_{s \in \mathcal{S}_I} n_y^R \int_s (H_{zh}^R E_{xh}^R - H_{zh}^L E_{xh}^L - H_{zh}^L E_{xh}^R + H_{zh}^L E_{xh}^L - H_{zh}^R E_{xh}^R + H_{zh}^L E_{xh}^R) \\ &+ \sum_{s \in \mathcal{S}_L} n_y^R \int_s (H_{zh}^R E_{xh}^R - H_{zh}^R E_{xh}^R) + \sum_{s \in \mathcal{S}_R} n_y^L \int_s (H_{zh}^L E_{xh}^L - H_{zh}^L E_{xh}^L) = 0, \end{aligned} \quad (27)$$

where  $\mathcal{S}_I$  denotes the set of all non-boundary sides,  $\mathcal{S}_L$  represents the set of sides on  $x = a$ , and  $\mathcal{S}_R$  on  $x = b$ . We can similarly deduce  $F_y = 0$ . We conclude the proof by integrate (24) over  $[0, t]$ .  $\square$

**Remark 3.1.** *The semi-discrete scheme satisfies the same energy conserving equality (23) as that of the model equation (22). We claim our method is energy conserving in this sense. The DG schemes with central flux also have this property [16]. Note that the famous upwind flux is dissipative and DG schemes equipped with it are not energy conserving.*

### 3.2 The error analysis

We denote the errors between the exact solutions  $(E_x, E_y, H_z, J_x, J_y, K_z)$  of (1)-(6) and the corresponding numerical solutions  $(E_{xh}, E_{yh}, H_{zh}, J_{xh}, J_{yh}, K_{zh})$  of the semi-discrete scheme (10)-(15) by

$$\mathcal{E}_x = E_x - E_{xh}, \mathcal{E}_y = E_y - E_{yh}, \mathcal{H}_z = H_z - H_{zh}, \mathcal{J}_x = J_x - J_{xh}, \mathcal{J}_y = J_y - J_{yh}, \mathcal{K}_z = K_z - K_{zh}. \quad (28)$$

Subtracting (10)-(15) from the weak formulation of (1)-(6) and assuming that the exact solutions are continuous in the domain  $\Omega$ , we can obtain the error equations:

$$\epsilon_0 \int_e \frac{\partial \mathcal{E}_x}{\partial t} \phi_x + \int_e \mathcal{H}_z \frac{\partial \phi_x}{\partial y} - \int_{\partial e} \hat{\mathcal{H}}_z \phi_x^{(in)} n_y^{(in)} + \int_e \mathcal{J}_x \phi_x = 0, \quad (29)$$

$$\epsilon_0 \int_e \frac{\partial \mathcal{E}_y}{\partial t} \phi_y - \int_e \mathcal{H}_z \frac{\partial \phi_y}{\partial x} + \int_{\partial e} \hat{\mathcal{H}}_z \phi_y^{(in)} n_x^{(in)} + \int_e \mathcal{J}_y \phi_y = 0, \quad (30)$$

$$\mu_0 \int_e \frac{\partial \mathcal{H}_z}{\partial t} \psi - \int_e \mathcal{E}_y \frac{\partial \psi}{\partial x} + \int_e \mathcal{E}_x \frac{\partial \psi}{\partial y} + \int_{\partial e} (\hat{\mathcal{E}}_y n_x^{(in)} - \hat{\mathcal{E}}_x n_y^{(in)}) \psi^{(in)} + \int_e \mathcal{K}_z \psi = 0, \quad (31)$$

$$\frac{1}{\epsilon_0 \omega_{pe}^2} \int_e \frac{\partial \mathcal{J}_x}{\partial t} u_1 + \frac{\Gamma_e}{\epsilon_0 \omega_{pe}^2} \int_e \mathcal{J}_x u_1 - \int_e \mathcal{E}_x u_1 = 0, \quad (32)$$

$$\frac{1}{\epsilon_0 \omega_{pe}^2} \int_e \frac{\partial \mathcal{J}_y}{\partial t} u_2 + \frac{\Gamma_e}{\epsilon_0 \omega_{pe}^2} \int_e \mathcal{J}_y u_2 - \int_e \mathcal{E}_y u_2 = 0, \quad (33)$$

$$\frac{1}{\mu_0 \omega_{pm}^2} \int_e \frac{\partial \mathcal{K}_z}{\partial t} v + \frac{\Gamma_m}{\mu_0 \omega_{pm}^2} \int_e \mathcal{K}_z v - \int_e \mathcal{H}_z v = 0. \quad (34)$$

**Theorem 3.2.** *Let  $(E_x, E_y, H_z, J_x, J_y, K_z)$  and  $(E_{xh}, E_{yh}, H_{zh}, J_{xh}, J_{yh}, K_{zh})$  be the solutions of (1)-(6) and (10)-(15), respectively. The following error estimate holds true:*

$$\begin{aligned} & \max_{0 \leq t \leq T} \left[ \epsilon_0 (||E_x - E_{xh}||^2 + ||E_y - E_{yh}||^2) + \mu_0 ||H_z - H_{zh}||^2 \right. \\ & \left. + \frac{1}{\epsilon_0 \omega_{pe}^2} (||J_x - J_{xh}||^2 + ||J_y - J_{yh}||^2) + \frac{1}{\mu_0 \omega_{pm}^2} ||K_z - K_{zh}||^2 \right] (t) \\ & \leq C T h^{2k} + C \left( \epsilon_0 (||E_x - E_{xh}||^2 + ||E_y - E_{yh}||^2) + \mu_0 ||H_z - H_{zh}||^2 \right) (0) \\ & \quad + C \left( \frac{1}{\epsilon_0 \omega_{pe}^2} (||J_x - J_{xh}||^2 + ||J_y - J_{yh}||^2) + \frac{1}{\mu_0 \omega_{pm}^2} ||K_z - K_{zh}||^2 \right) (0), \end{aligned}$$

where the constant  $C > 0$  is independent of  $h$ , and  $k \geq 1$  is the order of the basis function in  $V_h^k$ .

*Proof.* Using the defined projections, we can decompose the errors given in (28) as follows:

$$\begin{aligned} \mathcal{E}_x &= E_x - E_{xh} = (\Pi E_x - E_{xh}) - (\Pi E_x - E_x) := E_{x\xi} - E_{x\eta}, \\ \mathcal{E}_y &= E_y - E_{yh} = (\Pi E_y - E_{yh}) - (\Pi E_y - E_y) := E_{y\xi} - E_{y\eta}, \\ \mathcal{H}_z &= H_z - H_{zh} = (\Pi H_z - H_{zh}) - (\Pi H_z - H_z) := H_{z\xi} - H_{z\eta}, \end{aligned}$$

$$\begin{aligned}
\mathcal{J}_x &= J_x - J_{xh} = (\Pi J_x - J_{xh}) - (\Pi J_x - J_x) := J_{x\xi} - J_{x\eta}, \\
\mathcal{J}_y &= J_y - J_{yh} = (\Pi J_y - J_{yh}) - (\Pi J_y - J_y) := J_{y\xi} - J_{y\eta}, \\
\mathcal{K}_z &= K_z - K_{zh} = (\Pi K_z - K_{zh}) - (\Pi K_z - K_z) := K_{z\xi} - K_{z\eta}
\end{aligned}$$

where  $\Pi$  is the usual  $L^2$  projection onto  $V_h^k$ .

We denote the summation of (29) – (34) as:

$$B(\mathcal{E}_x, \mathcal{E}_y, \mathcal{H}_z, \mathcal{J}_x, \mathcal{J}_y, \mathcal{K}_z; \phi_x, \phi_y, \psi, u_1, u_2, v) = 0. \quad (35)$$

Substituting the error decomposition into (35), and choosing the test functions  $\phi_x = E_{x\xi}$ ,  $\phi_y = E_{y\xi}$ ,  $\psi = H_{z\xi}$ ,  $u_1 = J_{x\xi}$ ,  $u_2 = J_{y\xi}$ ,  $v = K_{z\xi}$ , we obtain:

$$\begin{aligned}
&B(E_{x\xi}, E_{y\xi}, H_{z\xi}, J_{x\xi}, J_{y\xi}, K_{z\xi}; E_{x\xi}, E_{y\xi}, H_{z\xi}, J_{x\xi}, J_{y\xi}, K_{z\xi}) \\
&= B(E_{x\eta}, E_{y\eta}, H_{z\eta}, J_{x\eta}, J_{y\eta}, K_{z\eta}; E_{x\xi}, E_{y\xi}, H_{z\xi}, J_{x\xi}, J_{y\xi}, K_{z\xi}).
\end{aligned} \quad (36)$$

If we sum (36) over all triangles and look at the left hand side (LHS), we could observe that it is exactly the same thing as in the stability proof. Hence we have:

$$\begin{aligned}
\text{LHS} &= \frac{1}{2} \frac{d}{dt} \left( \epsilon_0 (\|E_{x\xi}\|^2 + \|E_{y\xi}\|^2) + \mu_0 \|H_{z\xi}\|^2 + \frac{1}{\epsilon_0 \omega_{pe}^2} (\|J_{x\xi}\|^2 + \|J_{y\xi}\|^2) + \frac{1}{\mu_0 \omega_{pm}^2} \|K_{z\xi}\|^2 \right) \\
&\quad + \frac{2\Gamma_e}{\epsilon_0 \omega_{pe}^2} (\|J_{x\xi}\|^2 + \|J_{y\xi}\|^2) + \frac{2\Gamma_m}{\mu_0 \omega_{pm}^2} \|K_{z\xi}\|^2.
\end{aligned} \quad (37)$$

Now consider the terms on the right hand side (RHS). By the property of the projection  $\Pi u_t = (\Pi u)_t$ , and the fact that  $E_{x\xi}, E_{y\xi}, H_{z\xi}, J_{x\xi}, J_{y\xi}, K_{z\xi}|_e \in P_k(e)$ , we can have

$$\text{RHS} = \sum_{e \in \mathcal{T}_h} \int_{\partial e} \left( -\hat{H}_{z\eta} E_{x\xi}^{(in)} n_y^{(in)} + \hat{H}_{z\eta} E_{y\xi}^{(in)} n_x^{(in)} + \hat{E}_{y\eta} H_{z\xi}^{(in)} n_x^{(in)} - \hat{E}_{x\eta} H_{z\xi}^{(in)} n_y^{(in)} \right). \quad (38)$$

Let us focus on the first term:

$$\begin{aligned}
\sum_{e \in \mathcal{T}_h} \int_{\partial e} \hat{H}_{z\eta} E_{x\xi}^{(in)} n_y^{(in)} &\leq \sum_{e \in \mathcal{T}_h} \frac{1}{\delta h} \int_{\partial e} |\hat{H}_{z\eta}|^2 + \delta h \int_{\partial e} |E_{x\xi}^{(in)}|^2 \\
&\leq C \sum_{e \in \mathcal{T}_h} \left( \frac{1}{\delta} \|H_{z\eta}\|_{L^\infty(e)}^2 + \delta h^2 \|E_{x\xi}\|_{L^\infty(e)}^2 \right) \\
&\leq \frac{C}{\delta} h^{2k} \|H_z\|_{H^{k+1}(\Omega)}^2 + C\delta \|E_{x\xi}\|_{L^2(\Omega)}^2,
\end{aligned} \quad (39)$$

holds for any  $\delta > 0$ . The estimation of the first term is due to the approximating property of polynomial preserving operators (see Theorem 3.1.4 in [8]), and that of the second term can be justified by the standard inverse inequality [8]. Note that the constants are not necessarily the same, but are all written as  $C$  for brevity. The constants are all of course independent of the mesh sizes.

Treating the remaining terms in (38) similarly, we can get the following inequality:

$$\begin{aligned} & \frac{1}{2} \frac{d}{dt} \left( \epsilon_0 (\|E_{x\xi}\|^2 + \|E_{y\xi}\|^2) + \mu_0 \|H_{z\xi}\|^2 + \frac{1}{\epsilon_0 \omega_{pe}^2} (\|J_{x\xi}\|^2 + \|J_{y\xi}\|^2) + \frac{1}{\mu_0 \omega_{pm}^2} \|K_{z\xi}\|^2 \right) \\ & \leq \frac{C}{\delta} h^{2k} \left( \|E_x\|_{H^{k+1}(\Omega)}^2 + \|E_y\|_{H^{k+1}(\Omega)}^2 + \|H_z\|_{H^{k+1}(\Omega)}^2 \right) + C\delta (\|E_{x\xi}\|^2 + \|E_{y\xi}\|^2 + \|H_{z\xi}\|^2). \end{aligned} \quad (40)$$

Integrating (40) from  $t = 0$  to any  $t \leq T$ , we have

$$\begin{aligned} & \left( \epsilon_0 (\|E_{x\xi}\|^2 + \|E_{y\xi}\|^2) + \mu_0 \|H_{z\xi}\|^2 + \frac{1}{\epsilon_0 \omega_{pe}^2} (\|J_{x\xi}\|^2 + \|J_{y\xi}\|^2) + \frac{1}{\mu_0 \omega_{pm}^2} \|K_{z\xi}\|^2 \right) (t) \\ & - \left( \epsilon_0 (\|E_{x\xi}\|^2 + \|E_{y\xi}\|^2) + \mu_0 \|H_{z\xi}\|^2 + \frac{1}{\epsilon_0 \omega_{pe}^2} (\|J_{x\xi}\|^2 + \|J_{y\xi}\|^2) + \frac{1}{\mu_0 \omega_{pm}^2} \|K_{z\xi}\|^2 \right) (0) \\ & \leq \frac{C}{\delta} h^{2k} \int_0^t \left( \|E_x\|_{H^{k+1}(\Omega)}^2 + \|E_y\|_{H^{k+1}(\Omega)}^2 + \|H_z\|_{H^{k+1}(\Omega)}^2 \right) (s) ds \\ & + CT\delta \max_{0 \leq t \leq T} (\|E_{x\xi}\|^2 + \|E_{y\xi}\|^2 + \|H_{z\xi}\|^2) (t). \end{aligned} \quad (41)$$

Taking maximum of (41) with respect to time  $t$ , choosing  $\delta = o(\frac{1}{T})$  small enough so that the last term on the right hand side can be controlled by the LHS, and using the triangle inequality and the error estimate of  $L^2$  projections, we conclude the proof.  $\square$

**Remark 3.2.** *The suboptimal  $k$ -th order convergence rate in Theorem 3.2 is confirmed by the numerical results given in Table 1 below. The DG schemes with alternating flux and solution space  $Q_k$  in rectangular meshes [18] have optimal  $(k+1)$ -th order rate convergence. Note that  $Q_k = \{x^i y^j, i, j \in [0, k]\}$  and  $P_k = \{x^i y^j, i+j \in [0, k]\}$  and  $Q_k$  has almost twice as many degrees of freedom as  $P_k$  for large  $k$ . We implemented DG schemes with alternating flux and solution space  $P_k$  in rectangular meshes and they show suboptimal convergence rate too. The proof of optimal convergence rate in [18] heavily relies on the structure of  $Q_k$  and our numerical results show that it is indeed critical for optimality.*

**Remark 3.3.** *As we will see in Table 1, all variables except for  $H_z$  and  $K_z$  show the suboptimal convergence rate as in Theorem 3.2.  $H_z$  and  $K_z$  still has optimal convergence rates which is not fully reflected in Theorem 3.2.*

## 4 The fully-discrete DG method

We consider the following leap-frog LDG scheme: For any  $n \geq 0$ , find  $E_{xh}^{n+1}, E_{yh}^{n+1}, H_{zh}^{n+\frac{3}{2}}, J_{xh}^{n+\frac{3}{2}}, J_{yh}^{n+\frac{3}{2}}, K_{zh}^{n+2} \in V_h^k$  such that

$$\epsilon_0 \int_e \frac{E_{xh}^{n+1} - E_{xh}^n}{\tau} \phi_x - \int_{\partial e} \hat{H}_{zh}^{n+\frac{1}{2}} \phi_x^{(in)} n_y^{(in)} + \int_e H_{zh}^{n+\frac{1}{2}} \frac{\partial \phi_x}{\partial y} + \int_e J_{xh}^{n+\frac{1}{2}} \phi_x = 0, \quad (42)$$

$$\epsilon_0 \int_e \frac{E_{yh}^{n+1} - E_{yh}^n}{\tau} \phi_y + \int_{\partial e} \hat{H}_{zh}^{n+\frac{1}{2}} \phi_y^{(in)} n_x^{(in)} - \int_e H_{zh}^{n+\frac{1}{2}} \frac{\partial \phi_y}{\partial x} + \int_e J_{yh}^{n+\frac{1}{2}} \phi_y = 0, \quad (43)$$

$$\mu_0 \int_e \frac{H_{zh}^{n+\frac{3}{2}} - H_{zh}^{n+\frac{1}{2}}}{\tau} \psi + \int_{\partial e} \hat{E}_{yh}^{n+1} \psi^{(in)} n_x^{(in)} - \int_e E_{yh}^{n+1} \frac{\partial \psi}{\partial x} \quad (44)$$

$$- \int_{\partial e} \hat{E}_{xh}^{n+1} \psi^{(in)} n_y^{(in)} + \int_e E_{xh}^{n+1} \frac{\partial \psi}{\partial y} + \int_e K_{zh}^{n+1} \psi = 0,$$

$$\frac{1}{\epsilon_0 \omega_{pe}^2} \int_e \frac{J_{xh}^{n+\frac{3}{2}} - J_{xh}^{n+\frac{1}{2}}}{\tau} u_1 + \frac{\Gamma_e}{\epsilon_0 \omega_{pe}^2} \int_e \frac{J_{xh}^{n+\frac{3}{2}} + J_{xh}^{n+\frac{1}{2}}}{2} u_1 - \int_e E_{xh}^{n+1} u_1 = 0, \quad (45)$$

$$\frac{1}{\epsilon_0 \omega_{pe}^2} \int_e \frac{J_{yh}^{n+\frac{3}{2}} - J_{yh}^{n+\frac{1}{2}}}{\tau} u_2 + \frac{\Gamma_e}{\epsilon_0 \omega_{pe}^2} \int_e \frac{J_{yh}^{n+\frac{3}{2}} + J_{yh}^{n+\frac{1}{2}}}{2} u_2 - \int_e E_{yh}^{n+1} u_2 = 0, \quad (46)$$

$$\frac{1}{\mu_0 \omega_{pm}^2} \int_e \frac{K_{zh}^{n+2} - K_{zh}^{n+1}}{\tau} v + \frac{\Gamma_m}{\mu_0 \omega_{pm}^2} \int_e \frac{K_{zh}^{n+2} + K_{zh}^{n+1}}{2} v - \int_e H_{zh}^{n+\frac{3}{2}} v = 0, \quad (47)$$

for all test functions  $\phi_x, \phi_y, \psi, u_1, u_2, v \in V_h^k$ , with the following fluxes consistent with (16)-(21):

$$\hat{E}_{xh}^n = E_{xh}^{n,R} \quad (48)$$

$$\hat{E}_{yh}^n = E_{yh}^{n,R} \quad (49)$$

$$\hat{H}_{zh}^{n+\frac{1}{2}} = H_{zh}^{n+\frac{1}{2},L} \quad (50)$$

$$\hat{E}_{xh}^n = 0, \text{ on } y = c, d \quad (51)$$

$$\hat{E}_{yh}^n = 0, \text{ on } x = a, b \quad (52)$$

$$\hat{H}_{zh}^{n+\frac{1}{2}} = H_{zh}^{n+\frac{1}{2},(in)}, \text{ on } \partial\Omega. \quad (53)$$

With the above preparation, we can now prove the following stability. To shorten the notation, we introduce the vector  $L^2$  norm  $\|\mathbf{E}_h\|^2 = \|E_{xh}\|^2 + \|E_{yh}\|^2$  for vector  $\mathbf{E}_h = (E_{xh}, E_{yh})$ . Similar notation will be used for  $\|\mathbf{J}_h\|^2$  and  $\mathbf{J}_h$ . Any variable in the integration over the boundary of elements are by default the value taken from inside of the elements if not specified otherwise.

**Theorem 4.1.** Denote  $C_v = \frac{1}{\sqrt{\epsilon_0 \mu_0}}$  for the speed of light, and  $C_{inv}$  for the positive constant in the standard inverse estimate  $\|\frac{\partial u_h}{\partial i}\| \leq C_{inv} h^{-1} \|u_h\|$  for any  $u_h \in V_h^k$  and  $i = x, y$ . Under the assumption

$$\tau \leq \min\left(\frac{1}{2\omega_{pe}}, \frac{1}{2\omega_{pm}}, \frac{h}{2C_{inv}C_v}\right), \quad (54)$$

for any  $m \geq 1$  we have

$$\begin{aligned} & \epsilon_0 \|\mathbf{E}_h^{m+1}\|^2 + \mu_0 \|H_{zh}^{m+\frac{3}{2}}\|^2 + \frac{1}{\epsilon_0 \omega_{pe}^2} \|\mathbf{J}_h^{m+\frac{3}{2}}\|^2 + \frac{1}{\mu_0 \omega_{pm}^2} \|K_{zh}^{m+2}\|^2 \\ & \leq C \left( \epsilon_0 \|\mathbf{E}_h^0\|^2 + \mu_0 \|H_{zh}^{\frac{1}{2}}\|^2 + \frac{1}{\epsilon_0 \omega_{pe}^2} \|\mathbf{J}_h^{\frac{1}{2}}\|^2 + \frac{1}{\mu_0 \omega_{pm}^2} \|K_{zh}^1\|^2 \right), \end{aligned} \quad (55)$$

where the constant  $C > 1$  is independent of the mesh size  $h$  and the time step size  $\tau$ .

*Proof.* Choosing  $\phi_x = \tau(E_{xh}^{n+1} + E_{xh}^n)$ ,  $\phi_y = \tau(E_{yh}^{n+1} + E_{yh}^n)$ ,  $\psi = \tau(H_{zh}^{n+\frac{3}{2}} + H_{zh}^{n+\frac{1}{2}})$ ,  $u_1 = \tau(J_{xh}^{n+\frac{3}{2}} + J_{xh}^{n+\frac{1}{2}})$ ,  $u_2 = \tau(J_{yh}^{n+\frac{3}{2}} + J_{yh}^{n+\frac{1}{2}})$ ,  $v = \tau(K_{zh}^{n+2} + K_{zh}^{n+1})$  in (42)-(47), summing them up over elements

$e \in \mathcal{T}_h$ , and time levels  $0 \leq n \leq m$  for any  $m \geq 1$  we have:

$$\begin{aligned}
& \epsilon_0(\|\mathbf{E}_h^{m+1}\|^2 - \|\mathbf{E}_h^0\|^2) + \mu_0(\|H_{zh}^{m+\frac{3}{2}}\|^2 - \|H_{zh}^{\frac{1}{2}}\|^2) \\
& + \frac{1}{\epsilon_0\omega_{pe}^2}(\|\mathbf{J}_h^{m+\frac{3}{2}}\|^2 - \|\mathbf{J}_h^{\frac{1}{2}}\|^2) + \frac{1}{\mu_0\omega_{pm}^2}(\|K_{zh}^{m+2}\|^2 - \|K_{zh}^1\|^2) \\
& \leq \tau \int_{\Omega} \left( \mathbf{E}_h^{m+1} \cdot \mathbf{J}_h^{m+\frac{3}{2}} - \mathbf{E}_h^0 \cdot \mathbf{J}_h^{\frac{1}{2}} - H_{zh}^{m+\frac{3}{2}} K_{zh}^{m+2} + H_{zh}^{\frac{1}{2}} K_{zh}^1 \right) \\
& + F_0 + F_m + F_{x1} + F_{x2} - F_{y1} - F_{y2},
\end{aligned} \tag{56}$$

where the terms on the right hand side are:

$$\begin{aligned}
F_m &= \tau \sum_{e \in \mathcal{T}_h} \int_e \left( -E_{xh}^{m+1} \frac{\partial H_{zh}^{m+\frac{3}{2}}}{\partial y} + E_{yh}^{m+1} \frac{\partial H_{zh}^{m+\frac{3}{2}}}{\partial x} \right) + \int_{\partial e} \left( \hat{E}_{xh}^{m+1} H_{zh}^{m+\frac{3}{2}} n_y - \hat{E}_{yh}^{m+1} \hat{H}_{zh}^{m+\frac{3}{2}} n_x \right), \\
F_0 &= \tau \sum_{e \in \mathcal{T}_h} \int_e \left( -H_{zh}^{\frac{1}{2}} \frac{\partial E_{xh}^0}{\partial y} + H_{zh}^{\frac{1}{2}} \frac{\partial E_{yh}^0}{\partial x} \right) + \int_{\partial e} \left( \hat{H}_{zh}^{\frac{1}{2}} E_{xh}^0 n_y - \hat{H}_{zh}^{\frac{1}{2}} E_{yh}^0 n_x \right), \\
F_{x1} &= \tau \sum_{n=0}^m \sum_{e \in \mathcal{T}_h} \int_{\partial e} \left( \hat{H}_{zh}^{n+\frac{1}{2}} E_{xh}^{n+1} n_y + \hat{E}_{xh}^{n+1} H_{zh}^{n+\frac{1}{2}} n_y \right) + \int_e \left( -H_{zh}^{n+\frac{1}{2}} \frac{\partial E_{xh}^{n+1}}{\partial y} - E_{xh}^{n+1} \frac{\partial H_{zh}^{n+\frac{1}{2}}}{\partial y} \right), \\
F_{x2} &= \tau \sum_{n=1}^m \sum_{e \in \mathcal{T}_h} \int_{\partial e} \left( \hat{H}_{zh}^{n+\frac{1}{2}} E_{xh}^n n_y + \hat{E}_{xh}^n H_{zh}^{n+\frac{1}{2}} n_y \right) + \int_e \left( -H_{zh}^{n+\frac{1}{2}} \frac{\partial E_{xh}^n}{\partial y} - E_{xh}^n \frac{\partial H_{zh}^{n+\frac{1}{2}}}{\partial y} \right), \\
F_{y1} &= \tau \sum_{n=0}^m \sum_{e \in \mathcal{T}_h} \int_{\partial e} \left( \hat{H}_{zh}^{n+\frac{1}{2}} E_{yh}^{n+1} n_x + \hat{E}_{yh}^{n+1} H_{zh}^{n+\frac{1}{2}} n_x \right) + \int_e \left( -H_{zh}^{n+\frac{1}{2}} \frac{\partial E_{yh}^{n+1}}{\partial x} - E_{yh}^{n+1} \frac{\partial H_{zh}^{n+\frac{1}{2}}}{\partial x} \right), \\
F_{y2} &= \tau \sum_{n=1}^m \sum_{e \in \mathcal{T}_h} \int_{\partial e} \left( \hat{H}_{zh}^{n+\frac{1}{2}} E_{yh}^n n_x + \hat{E}_{yh}^n H_{zh}^{n+\frac{1}{2}} n_x \right) + \int_e \left( -H_{zh}^{n+\frac{1}{2}} \frac{\partial E_{yh}^n}{\partial x} - E_{yh}^n \frac{\partial H_{zh}^{n+\frac{1}{2}}}{\partial x} \right).
\end{aligned}$$

We cancel the flux terms similarly to (27) in the proof of Theorem 3.1 and get:

$$F_{x1} = 0, F_{x2} = 0, F_{y1} = 0, F_{y2} = 0. \tag{57}$$

By using the Cauchy-Schwartz inequality, we have:

$$\begin{aligned}
& \tau \int_{\Omega} \left( \mathbf{E}_h^{m+1} \cdot \mathbf{J}_h^{m+\frac{3}{2}} - \mathbf{E}_h^0 \cdot \mathbf{J}_h^{\frac{1}{2}} - H_{zh}^{m+\frac{3}{2}} K_{zh}^{m+2} + H_{zh}^{\frac{1}{2}} K_{zh}^1 \right) \\
& \leq \frac{\tau\omega_{pe}}{2} \left( \frac{1}{\epsilon_0\omega_{pe}^2} \|\mathbf{J}_h^{\frac{1}{2}}\|^2 + \epsilon_0 \|\mathbf{E}_h^0\|^2 \right) + \frac{\tau\omega_{pe}}{2} \left( \frac{1}{\epsilon_0\omega_{pe}^2} \|\mathbf{J}_h^{m+\frac{3}{2}}\|^2 + \epsilon_0 \|\mathbf{E}_h^{m+1}\|^2 \right) \\
& + \frac{\tau\omega_{pm}}{2} \left( \frac{1}{\mu_0\omega_{pm}^2} \|K_{zh}^1\|^2 + \mu_0 \|H_{zh}^{\frac{1}{2}}\|^2 \right) + \frac{\tau\omega_{pm}}{2} \left( \frac{1}{\mu_0\omega_{pm}^2} \|K_{zh}^{m+2}\|^2 + \mu_0 \|H_{zh}^{m+\frac{3}{2}}\|^2 \right).
\end{aligned} \tag{58}$$

We utilize the inverse inequality along with Cauchy-Schwarz inequality to estimate  $F_m + F_0$ :

(similar to the proof of Theorem 3.2.6 in [8])

$$\begin{aligned}
F_0 + F_m \leq & \tau \cdot \frac{C_{inv}C_v}{2h} \left( \epsilon_0 \|E_{xh}^{m+1}\|^2 + \mu_0 \|H_{zh}^{m+\frac{3}{2}}\|^2 + \epsilon_0 \|E_{xh}^0\|^2 + \mu_0 \|H_{zh}^{\frac{1}{2}}\|^2 \right) \\
& + \tau \cdot \frac{C_{inv}C_v}{2h} \left( \epsilon_0 \|E_{yh}^{m+1}\|^2 + \mu_0 \|H_{zh}^{m+\frac{3}{2}}\|^2 + \epsilon_0 \|E_{yh}^0\|^2 + \mu_0 \|H_{zh}^{\frac{1}{2}}\|^2 \right).
\end{aligned} \tag{59}$$

The proof is concluded by substituting (57)–(59) into (56) and applying assumption (54) in the above inequality.  $\square$

**Remark 4.1.** *Under the same assumption as Theorem 4.1 coupled with the assumptions on the initial value:*

$$\epsilon_0 \|\mathbf{E}^0 - \mathbf{E}_h^0\|^2 + \mu_0 \|H_z^{\frac{1}{2}} - H_{zh}^{\frac{1}{2}}\|^2 + \frac{1}{\epsilon_0 \omega_{pe}^2} \|\mathbf{J}^{\frac{1}{2}} - \mathbf{J}_h^{\frac{1}{2}}\|^2 + \frac{1}{\mu_0 \omega_{pm}^2} \|K_z^1 - K_{zh}^1\|^2 \leq Ch^{2k},$$

we can prove the following error estimate: for any  $m \geq 1$

$$\begin{aligned}
& \epsilon_0 \|\mathbf{E}^{m+1} - \mathbf{E}_h^{m+1}\|^2 + \mu_0 \|H_z^{m+\frac{3}{2}} - H_{zh}^{m+\frac{3}{2}}\|^2 \\
& + \frac{1}{\epsilon_0 \omega_{pe}^2} \|\mathbf{J}^{m+\frac{3}{2}} - \mathbf{J}_h^{m+\frac{3}{2}}\|^2 + \frac{1}{\mu_0 \omega_{pm}^2} \|K_z^{m+2} - K_{zh}^{m+2}\|^2 \leq C (h^k + \tau^2)^2.
\end{aligned}$$

The proof can be carried out by following the similar idea to the proofs of Theorems 3.2 and 4.1 coupled with time discretization estimates (cf. [17, Ch.3]).

## 5 Numerical results

In this section we present the error tables, and two interesting simulations showing the backward wave propagation across the interface of vacuum and metamaterial. For the error tables, we construct exact solutions for the following system of equations with added source terms and  $\omega$  being 2.

$$\frac{\partial E_x}{\partial t} = \frac{\partial H_z}{\partial y} - J_x + f_x, \tag{60}$$

$$\frac{\partial E_y}{\partial t} = -\frac{\partial H_z}{\partial x} - J_y + f_y, \tag{61}$$

$$\frac{\partial H_z}{\partial t} = -\frac{\partial E_y}{\partial x} + \frac{\partial E_x}{\partial y} - K_z + g, \tag{62}$$

$$\frac{1}{\omega^2 \pi^2} \frac{\partial J_x}{\partial t} = -\frac{2}{\omega \pi} J_x + E_x, \tag{63}$$

$$\frac{1}{\omega^2 \pi^2} \frac{\partial J_y}{\partial t} = -\frac{2}{\omega \pi} J_y + E_y, \tag{64}$$

$$\frac{1}{\omega^2 \pi^2} \frac{\partial K_z}{\partial t} = -\frac{2}{\omega \pi} K_z + H_z, \tag{65}$$

and the exact solutions are:

$$E_x(x, y, t) = \cos(\omega \pi x) \sin(\omega \pi y) e^{-\omega \pi t}, \tag{66}$$

$$E_y(x, y, t) = -\sin(\omega\pi x) \cos(\omega\pi y) e^{-\omega\pi t}, \quad (67)$$

$$H_z(x, y, t) = \cos(\omega\pi x) \cos(\omega\pi y) e^{-\omega\pi t}, \quad (68)$$

$$J_x(x, y, t) = \omega\pi E_x, \quad J_y = \omega\pi E_y, \quad K_z = \omega\pi H_z \quad (69)$$

with corresponding source terms:

$$f_x = J_x, \quad f_y = J_y, \quad g = -2\omega\pi H_z. \quad (70)$$

### 5.1 Error table with leap-frog time stepping

We implement the leap-frog scheme (42)–(47) with alternating flux (48)–(53) and polynomial space of degree 2. The  $L^2$  error and error rate for each variable is shown in Table 1. The error is evaluated at  $T = 0.1$ . For the purpose of showing the suboptimal convergence rate, we choose  $\Delta t = 0.05h^{\frac{3}{2}}$  so that the error from time stepping would be  $O(h^3)$ . In Table 1, we can see that the space error of  $\mathbf{E}$  and  $\mathbf{J}$  is of second order and dominates the time error. To compare our results with existing work using the central flux [16]:

$$\hat{E}_{xh} = \frac{1}{2} (E_{xh}^R + E_{xh}^L), \quad \hat{E}_{yh} = \frac{1}{2} (E_{yh}^R + E_{yh}^L), \quad \hat{H}_{zh} = \frac{1}{2} (H_{zh}^R + H_{zh}^L)$$

instead of our alternating flux (16)–(18), we implement the same scheme with the flux replaced by the central flux and get similar results shown in Table 2.

As discussed in Remark 3.2, the alternating flux is optimal for DG schemes with  $Q_k$  solution spaces on rectangular meshes while the central flux is suboptimal. It appears that, for DG schemes on triangular meshes with  $P_k$  solution spaces, these two fluxes are rather similar in terms of convergence rates.

Table 1: Leap-frog, alternating flux,  $P_2$  basis function,  $T = 0.1$ ,  $\Delta t = 0.05h^{\frac{3}{2}}$

Level of Refinement	Error of $E_x$		Error of $E_y$		Error of $H_z$	
	$L^2$ Error	Order	$L^2$ Error	Order	$L^2$ Error	Order
1	8.42e-03	-inf	9.91e-03	-inf	6.37e-03	-inf
2	1.68e-03	2.33	2.45e-03	2.01	8.72e-04	2.87
3	3.65e-04	2.20	5.93e-04	2.05	1.01e-04	3.10
4	8.57e-05	2.09	1.46e-04	2.02	1.36e-05	2.90
5	2.08e-05	2.04	3.65e-05	2.00	1.85e-06	2.88
Level of Refinement	Error of $J_x$		Error of $J_y$		Error of $K_z$	
	$L^2$ Error	Order	$L^2$ Error	Order	$L^2$ Error	Order
1	1.92e-02	-inf	2.09e-02	-inf	1.63e-02	-inf
2	3.00e-03	2.68	4.09e-03	2.35	2.31e-03	2.82
3	5.90e-04	2.35	9.19e-04	2.15	2.79e-04	3.05
4	1.32e-04	2.16	2.22e-04	2.05	3.49e-05	3.00
5	3.15e-05	2.06	5.49e-05	2.02	4.38e-06	2.99

Table 2: Leap-frog, central flux,  $P_2$  basis function,  $T = 0.1$ ,  $\Delta t = 0.05h^{\frac{3}{2}}$

Level of Refinement	Error of $E_x$		Error of $E_y$		Error of $H_z$	
	$L^2$ Error	Order	$L^2$ Error	Order	$L^2$ Error	Order
1	8.36e-03	-inf	8.36e-03	-inf	7.84e-03	-inf
2	1.44e-03	2.54	1.44e-03	2.54	7.63e-04	3.36
3	3.01e-04	2.26	3.01e-04	2.26	9.61e-05	2.99
4	7.17e-05	2.07	7.17e-05	2.07	1.05e-05	3.19
5	1.76e-05	2.02	1.76e-05	2.02	1.27e-06	3.04
Level of Refinement	Error of $J_x$		Error of $J_y$		Error of $K_z$	
	$L^2$ Error	Order	$L^2$ Error	Order	$L^2$ Error	Order
1	2.05e-02	-inf	2.05e-02	-inf	1.73e-02	-inf
2	2.83e-03	2.86	2.83e-03	2.86	2.06e-03	3.07
3	5.10e-04	2.47	5.10e-04	2.47	2.61e-04	2.98
4	1.11e-04	2.20	1.11e-04	2.20	3.23e-05	3.01
5	2.67e-05	2.06	2.67e-05	2.06	4.03e-06	3.00

## 5.2 Error table with Runge-Kutta time stepping

In this section we implement one more flux, the upwind flux, and further compare the convergence rate between fluxes. For the ease of implementation, we used the Runge-Kutta time stepping, see e.g. [10]. As shown in Table 3, the upwind flux produces optimal convergence rate. DG schemes with alternating and central fluxes still show suboptimal convergence rates in Tables 4 and 5.

Table 3: Runge-Kutta, upwind flux,  $P_2$  basis function,  $T = 0.1$ ,  $\Delta t = 0.05h$

Level of Refinement	Error of $E_x$		Error of $E_y$		Error of $H_z$	
	$L^2$ Error	Order	$L^2$ Error	Order	$L^2$ Error	Order
1	4.83e-03	-	4.83e-03	-	3.67e-03	-
2	5.03e-04	3.27	5.03e-04	3.27	4.33e-04	3.08
3	5.85e-05	3.10	5.85e-05	3.10	5.14e-05	3.07
4	7.07e-06	3.05	7.07e-06	3.05	6.28e-06	3.03
5	8.69e-07	3.02	8.69e-07	3.02	7.80e-07	3.01
Level of Refinement	Error of $J_x$		Error of $J_y$		Error of $K_z$	
	$L^2$ Error	Order	$L^2$ Error	Order	$L^2$ Error	Order
1	1.71e-02	-	1.71e-02	-	1.63e-02	-
2	2.11e-03	3.02	2.11e-03	3.02	2.01e-03	3.02
3	2.65e-04	2.99	2.65e-04	2.99	2.50e-04	3.00
4	3.30e-05	3.01	3.30e-05	3.01	3.11e-05	3.01
5	4.11e-06	3.00	4.11e-06	3.00	3.87e-06	3.00

Table 4: Runge-Kutta, alternating flux,  $P_2$  basis function,  $T = 0.1$ ,  $\Delta t = 0.05h$

Level of Refinement	Error of $E_x$		Error of $E_y$		Error of $H_z$	
	$L^2$ Error	Order	$L^2$ Error	Order	$L^2$ Error	Order
1	8.17e-03	–	9.85e-03	–	5.76e-03	–
2	1.65e-03	2.31	2.43e-03	2.02	7.95e-04	2.86
3	3.61e-04	2.19	5.92e-04	2.04	9.19e-05	3.11
4	8.58e-05	2.08	1.46e-04	2.02	1.14e-05	3.01
5	2.08e-05	2.04	3.65e-05	2.00	1.48e-06	2.94

Level of Refinement	Error of $J_x$		Error of $J_y$		Error of $K_z$	
	$L^2$ Error	Order	$L^2$ Error	Order	$L^2$ Error	Order
1	1.93e-02	–	2.08e-02	–	1.66e-02	–
2	2.99e-03	2.69	4.05e-03	2.36	2.32e-03	2.84
3	5.87e-04	2.35	9.15e-04	2.15	2.80e-04	3.05
4	1.31e-04	2.16	2.22e-04	2.05	3.50e-05	3.00
5	3.15e-05	2.06	5.49e-05	2.01	4.38e-06	3.00

Table 5: Runge-Kutta, central flux,  $P_2$  basis function,  $T = 0.1$ ,  $\Delta t = 0.05h$

Level of Refinement	Error of $E_x$		Error of $E_y$		Error of $H_z$	
	$L^2$ Error	Order	$L^2$ Error	Order	$L^2$ Error	Order
1	8.20e-03	–	8.20e-03	–	7.85e-03	–
2	1.44e-03	2.51	1.44e-03	2.51	7.50e-04	3.39
3	3.00e-04	2.26	3.00e-04	2.26	9.14e-05	3.04
4	7.15e-05	2.07	7.15e-05	2.07	9.55e-06	3.26
5	1.76e-05	2.02	1.76e-05	2.02	1.08e-06	3.15

Level of Refinement	Error of $J_x$		Error of $J_y$		Error of $K_z$	
	$L^2$ Error	Order	$L^2$ Error	Order	$L^2$ Error	Order
1	2.06e-02	–	2.06e-02	–	1.75e-02	–
2	2.82e-03	2.87	2.82e-03	2.87	2.08e-03	3.07
3	5.08e-04	2.47	5.08e-04	2.47	2.61e-04	2.99
4	1.11e-04	2.19	1.11e-04	2.19	3.23e-05	3.02
5	2.67e-05	2.06	2.67e-05	2.06	4.03e-06	3.00

### 5.3 Wave propagation in a rectangular metamaterial slab

One of the advantage of triangular meshes over the rectangular meshes is the flexibility in the shape of physical domains they can model. In this section we consider a rectangular region with a triangular metamaterial slab located inside a vacuum as in [16]. To absorb the outgoing waves, we wrap the whole region by a perfectly matched layer (PML).

In the mesh visualization (Figure 1) the blue triangle, with vertices  $(0.024, 0.002)$ ,  $(0.054, 0.002)$ , and  $(0.024, 0.062)$ , consists of the metamaterial. The red area, a rectangle  $[0, 0.07] \times [0, 0.064]$ , represents the vacuum. The green band with thickness  $dd = 2.4 \times 10^{-3}$  on the boundary is the PML.

The equation in the metamaterial is the Drude model (1)–(6), with  $\Gamma_e = \Gamma_m = 1 \times 10^8$ ,  $\mu_0 = 4\pi \times 10^{-7}$ ,  $c_v = 3 \times 10^8$ ,  $\epsilon_0 = 1/(c_v^2 \mu_0)$ ,  $w_{pe} = w_{pm} = 2\sqrt{2}\pi$ . Those in the vacuum are the usual Maxwell's equations. The PML equations we used are the following [16]:

$$\epsilon_0 \frac{\partial E_x}{\partial t} = \epsilon_0(\sigma_x - \sigma_y)E_x + \frac{\partial H_z}{\partial y} - J_x, \quad (71)$$

$$\epsilon_0 \frac{\partial E_y}{\partial t} = \epsilon_0(\sigma_y - \sigma_x)E_y - \frac{\partial H_z}{\partial x} - J_y, \quad (72)$$

$$\mu_0 \frac{\partial H_z}{\partial t} = -\mu_0(\sigma_x + \sigma_y)H_z + \frac{\partial E_x}{\partial y} - \frac{\partial E_y}{\partial x} - K_z, \quad (73)$$

$$\frac{\partial J_x}{\partial t} = -\sigma_x J_x + \epsilon_0(\sigma_x - \sigma_y)\sigma_x E_x, \quad (74)$$

$$\frac{\partial J_y}{\partial t} = -\sigma_y J_y + \epsilon_0(\sigma_y - \sigma_x)\sigma_y E_y, \quad (75)$$

$$\frac{\partial K_z}{\partial t} = \mu_0 \sigma_x \sigma_y H_z, \quad (76)$$

where

$$\sigma_x(x, y) = \begin{cases} \sigma_m \left(\frac{x-0.07}{dd}\right)^4, & x \geq 0.07, \\ \sigma_m (x/dd)^4, & x \leq 0, \\ 0, & \text{otherwise,} \end{cases} \quad (77)$$

with  $\sigma_m = -\log(err) * 5 * 0.07 * c_v / (2 * dd)$  and  $err = 10^{-7}$ .  $\sigma_y$  has the same form with  $x$  replaced by  $y$ . The initial condition is zero in the whole region, and the wave is incited by a source wave

$$e^{-10000(y-0.03)^2} f(t)$$

imposed on the line of  $x = 0.004$  and  $y \in [0.025, 0.035]$  to the  $H_z$  field. Here  $f$  is defined as

$$f(t) = \begin{cases} 0, & t < 0 \\ g_1(t) \sin(\omega_0 t), & 0 < t < mT_p \\ \sin(\omega_0 t), & mT_p < t < (m+k)T_p \\ g_2(t) \sin(\omega_0 t), & (m+k)T_p < t < (2m+k)T_p \\ 0, & t > (2m+k)T_p, \end{cases}$$

where  $\omega_0 = 2\pi f_0$ ,  $T_p = 1/f_0$ ,  $f_0 = 3 \times 10^8$ ,  $m = 2$ ,  $k = 100$ , and

$$g_1(t) = 10x_1^3 - 15x_1^4 + 6x_1^5, \text{ with } x_1 = t/mT_p, \\ g_2(t) = 1 - 10x_2^3 - 15x_2^4 + 6x_2^5, \text{ with } x_2 = t - (m+k)T_p/mT_p.$$

We use a time step  $\tau = 0.1$  ps and plot the  $H_z$  field at 1000, 2000, 3000, 4000, and 5000 time steps in Figures 2–6, showing results consistent with the simulation in [16].

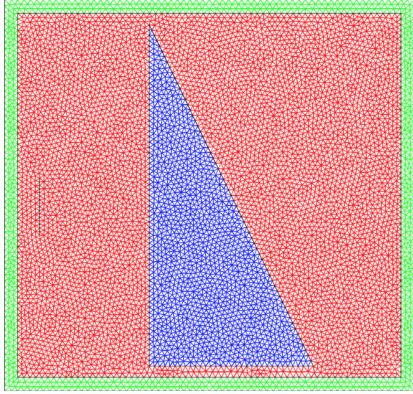


Figure 1: Mesh of triangular slab in vacuum

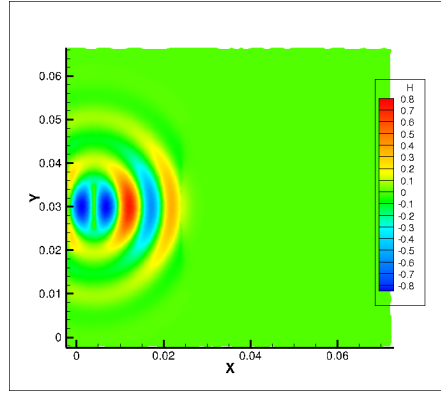


Figure 2:  $H_z$  value at 1000 time step

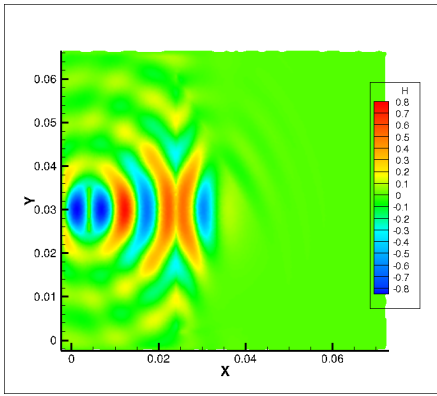


Figure 3:  $H_z$  value at 2000 time step

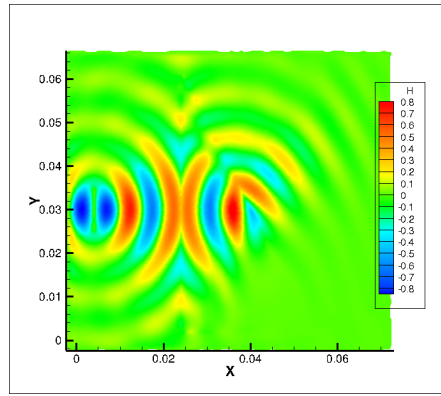


Figure 4:  $H_z$  value at 3000 time step

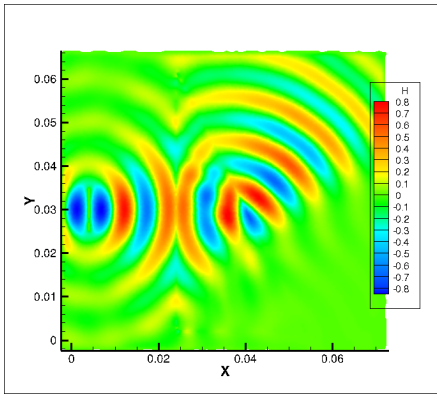


Figure 5:  $H_z$  value at 4000 time step

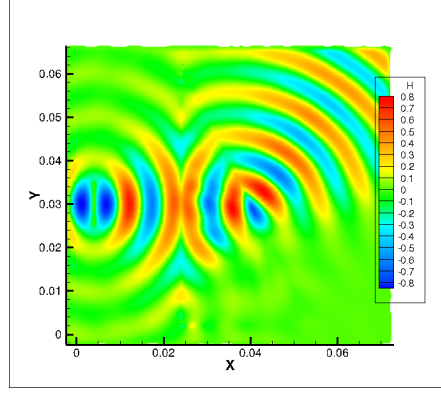


Figure 6:  $H_z$  value at 5000 time step

#### 5.4 Wave propagation in a rectangular metamaterial slab

We replace the triangular slab of metamaterial in the previous section by a rectangular one  $[0.024, 0.054] \times [0.002, 0.062]$ , and obtain snapshots of  $H_z$  shown in Figures 7–12. Again, our results

are consistent with the simulation obtained in [16].

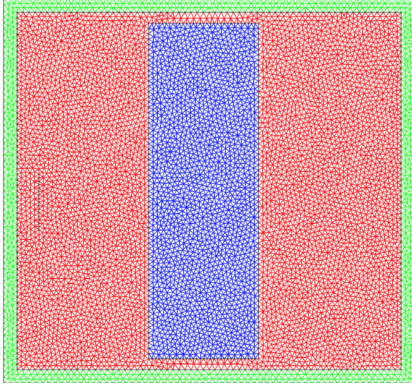


Figure 7: Mesh of triangular slab in vacuum

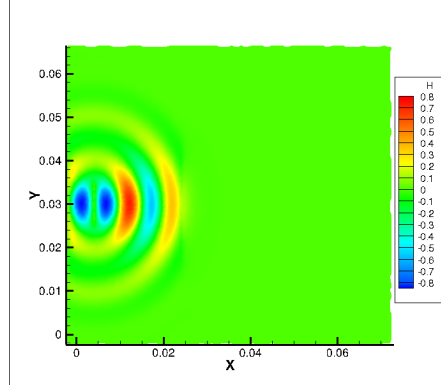


Figure 8:  $H_z$  value at 1000 time step

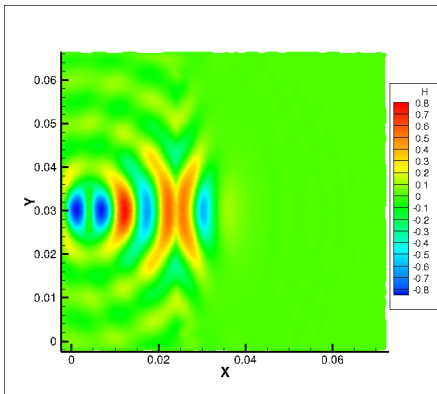


Figure 9:  $H_z$  value at 2000 time step

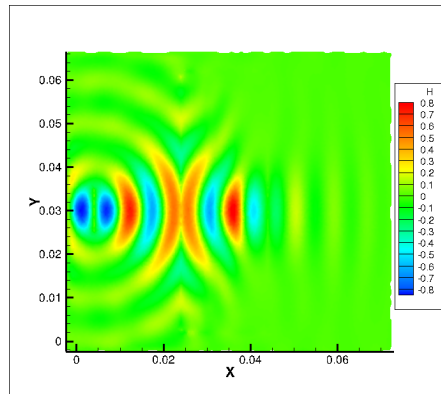


Figure 10:  $H_z$  value at 3000 time step

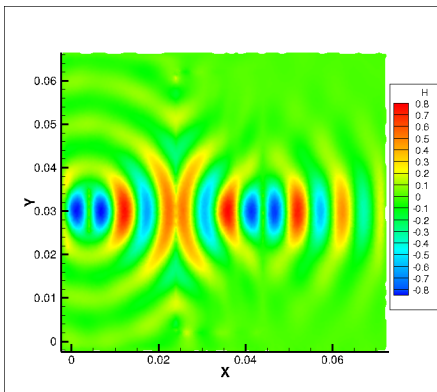


Figure 11:  $H_z$  value at 4000 time step

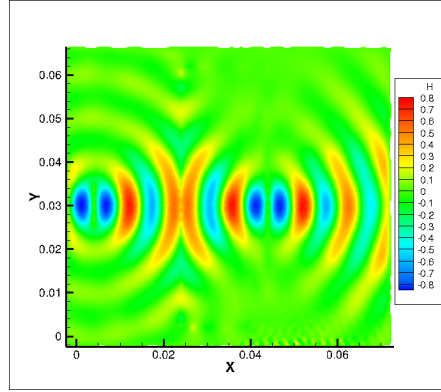


Figure 12:  $H_z$  value at 5000 time step

## 6 Conclusion

We present the DG methods with alternating fluxes on triangular meshes which only have suboptimal convergence rates. We postulate that the suboptimality is inherent in the  $P_k$  solution space. We prove the energy conservation and an error estimate for the semi-discrete schemes. The stability of the fully discrete scheme is proved and its error estimate is stated. We present convergence rate tables which are consistent with our theoretical error estimate, and simulation of backward wave propagation in Drude metamaterials to demonstrate the flexibility of triangular meshes.

## References

- [1] A.A. Basharin, M. Kafesaki, E.N. Economou and C.M. Soukoulis, Backward wave radiation from negative permittivity waveguides and its use for THz sub-wavelength imaging, *Optics Express* 20 (2012) 12752-12760.
- [2] S.C. Brenner, J. Gedicke and L.-Y. Sung, An adaptive P1 finite element method for two-dimensional transverse magnetic time harmonic Maxwell's equations with general material properties and general boundary conditions, *J. Sci. Comput.* 68 (2016) 848-863.
- [3] A. Buffa, P. Houston and I. Perugia, Discontinuous Galerkin computation of the Maxwell eigenvalues on simplicial meshes, *J. Comput. Appl. Math.* 204 (2007) 317-333.
- [4] M. Cassier, P. Joly and M. Kachanovska, Mathematical models for dispersive electromagnetic waves: An overview, *Comput. Math. Appl.* 74 (2017) 2792-2830.
- [5] H. Chen and M. Chen, Flipping photons backward: reversed Cherenkov radiation, *Mater. Today* 14 (2011) 34-41.
- [6] E.T. Chung and P. Ciarlet Jr., A staggered discontinuous Galerkin method for wave propagation in media with dielectrics and meta-materials, *J. Comput. Appl. Math.* 239 (2013) 189-207.
- [7] E.T. Chung, Q. Du and J. Zou, Convergence analysis of a finite volume method for Maxwell's equations in nonhomogeneous media, *SIAM J. Numer. Anal.* 41 (2003) 37-63.
- [8] P.G. Ciarlet, *Finite Element Method for Elliptic Problems*. SIAM, Philadelphia, 2002.
- [9] B. Cockburn and C.-W. Shu, TVB Runge-Kutta local projection discontinuous Galerkin finite element method for conservation laws II: general framework, *Math. Comp.* 52 (1989) 411-435.
- [10] B. Cockburn and C.-W. Shu, The Runge-Kutta discontinuous Galerkin method for conservation laws V: multidimensional systems, *J. Comput. Phys.* 141 (1998) 199-224.
- [11] B. Cockburn and C.-W. Shu, The local discontinuous Galerkin method for time-dependent convection-diffusion systems, *SIAM J. Numer. Anal.* 35 (1998) 2240-2463.
- [12] B. Cockburn and C.-W. Shu, Runge-Kutta discontinuous Galerkin methods for convection-dominated problems, *J. Sci. Comput.* 16 (2001) 173-261.
- [13] L. Demkowicz, J. Kurtz, D. Pardo, M. Paszynski, W. Rachowicz and A. Zdunek, *Computing with hp-Adaptive Finite Elements. Vol.2: Frontiers: Three Dimensional Elliptic and Maxwell Problems with Applications*. Chapman & Hall/CRC, 2008.
- [14] Z.Y. Duan, B.I. Wu, S. Xi, H.S. Chen and M. Chen, Research progress in reversed Cherenkov radiation in double-negative metamaterials, *Prog Electromagn Res* 90 (2009) 75-87.
- [15] J.S. Hesthaven and T. Warburton, *Nodal Discontinuous Galerkin Methods: Algorithms, Analysis, and Applications*. Springer, New York, 2008.
- [16] J. Li and J.S. Hesthaven, Analysis and application of the nodal discontinuous Galerkin method for wave propagation in metamaterials, *J. Comput. Phys.* 258 (2014) 915-930.

- [17] J. Li and Y. Huang, *Time-Domain Finite Element Methods for Maxwell's Equations in Metamaterials*. Springer Berlin Heidelberg, 2013.
- [18] J. Li, C. Shi and C.-W. Shu, Optimal non-dissipative discontinuous Galerkin methods for Maxwell's equations in Drude metamaterials, *Comput. Math. Appl.* 73 (2017) 1768-1780.
- [19] W. Li, D. Liang and Y. Lin, Symmetric energy-conserved S-FDTD scheme for two-dimensional Maxwell's equations in negative index metamaterials, *J. Sci. Comput.* 69 (2016) 696-735.
- [20] P. Monk, *Finite Element Methods for Maxwell's Equations*. Oxford University Press, 2003.
- [21] L. Mu, J. Wang, X. Ye and S. Zhang, A weak Galerkin finite element method for the Maxwell equations, *J. Sci. Comput.* 65 (2015) 363-386.
- [22] W.H. Reed and T.R. Hill, *Triangular mesh methods for the neutron transport equation*. Tech. Report LA-UR-73-479, Los Alamos Scientific Laboratory, 1973.
- [23] D.R. Smith, W.J. Padilla, D.C. Vier, S.C. Nemat-Nasser and S. Schultz, Composite medium with simultaneously negative permeability and permittivity, *Phys. Rev. Lett.* 84 (2000) 4184-4187.
- [24] J. Wang, Z. Xie and C. Chen, Implicit DG method for time domain maxwell's equations involving metamaterials, *Adv. Appl. Math. Mech.* 7 (2015) 796-817.
- [25] C.M. Watts, X.L. Liu and W.J. Padilla, Metamaterial electromagnetic wave absorbers, *Advanced Materials* 24 (2012) OP98-OP120
- [26] Y. Xing, C.-S. Chou and C.-W. Shu, Energy conserving local discontinuous Galerkin methods for wave propagation problems, *Inverse Probl. Imag.* 7 (2013) 967-986.
- [27] Y. Xu and C.-W. Shu, Local discontinuous Galerkin methods for high-order time-dependent partial differential equations, *Commun. Comput. Phys.* 7 (2010) 1-46.
- [28] Z. Yang, L.-L. Wang, Z. Rong, B. Wang and B. Zhang, Seamless integration of global Dirichlet-to-Neumann boundary condition and spectral elements for transformation electromagnetics, *Comput. Methods Appl. Mech. Engrg.* 301 (2016) 137-163.
- [29] S. Zhang, C.G. Xia and N. Fang, Broadband acoustic cloak for ultrasound waves, *Phys. Rev. Lett.* 106 (2011) 024301.
- [30] L. Zhong, L. Chen, S. Shu, G. Wittum and J. Xu, Quasi-optimal convergence of adaptive edge finite element methods for three dimensional indefinite time-harmonic Maxwell's equations, *Math. Comp.* 81 (278) 623-642.